Geophysical Research Letters

RESEARCH LETTER
10.1029/2024GL111981

Special Collection:
Space Weather Events of 2024 May 9-15

Imaging the May 2024 Extreme Aurora With Ionospheric Total Electron Content

J. C. Foster[1], P. J. Erickson[1], Y. Nishimura[2], S. R. Zhang[1], D. C. Bush[3], A. J. Coster[1], P. E. Meade[4], and E. Franco-Diaz[4]

[1]Haystack Observatory, Massachusetts Institute of Technology, Westford, MA, USA, [2]Department of Electrical and Computer Engineering and Center for Space Physics, Boston University, Boston, MA, USA, [3]Missouri Skies Observatory, Albany, MO, USA, [4]Computational Physics Inc., Lafayette, CO, USA

Abstract The continental United States is well instrumented with facilities for mid-latitude upper atmosphere research that operate on a continuous basis. In addition, citizen scientists provide a wealth of information when unusual events occur. We combine ionospheric total electron content (TEC) data from distributed arrays of GNSS receivers, magnetometer chains, and auroral observations obtained by citizen scientists, to provide a detailed view of the intense auroral breakup and westward surge occurring at the peak of the 10–11 May 2024 extreme geomagnetic storm. Over a 20-min interval, vertical TEC (vTEC) increased at unusually low latitude (~45°) and rapidly expanded azimuthally across the continent. Individual receiver/satellite data sets indicate sharp bursts of greatly elevated of vTEC (~50 TECu). Intense red aurora was co-located with the leading edge of the equatorward and westward TEC enhancements, indicating that the large TEC enhancement was created by extremely intense low-energy precipitation during the rapid substorm breakup.

Plain Language Summary For over 12 hr, the 10–11 May 2024 the extreme Gannon geomagnetic storm sent brilliant auroral displays into the night skies at mid and low latitudes around the world. Precipitating auroral electrons and protons ionize the upper atmosphere at 100–500 km altitude, increasing ionospheric total electron content (TEC). We use the perturbation of the signals received by the distributed array of navigation satellite receivers to map the intensification and spread of an extreme auroral event across the continental US. Photo and video observations of the auroral event contributed by citizen scientists indicate that the TEC enhancement closely matched the westward and equatorward expansion of strong red aurora. Coincident with the auroral breakup, sharp bursts of greatly elevated TEC were observed. Auroral breakup was accompanied by a bright red over green discrete auroral feature at the leading edge of the equatorward expansion of strong red aurora. Based on the direct auroral observations, we believe that the westward expansion of low-energy electron precipitation is likely the driver of the large TEC enhancements observed during the event.

Key Points:

- Total electron content (TEC) maps show the intensification and spread of the 11 May 2024 extreme auroral event across the continental US over a 20-min interval
- All sky camera imagery indicates that the TEC enhancement closely matches the westward and equatorward expansion of strong red aurora
- Coincident with auroral breakup, individual receiver/satellite data sets show sharp bursts of greatly elevated TEC 50 TECu above background

Supporting Information:

Supporting Information may be found in the online version of this article.

Correspondence to:

J. C. Foster,
jcfoster@mit.edu

Citation:

Foster, J. C., Erickson, P. J., Nishimura, Y., Zhang, S. R., Bush, D. C., Coster, A. J., et al. (2024). Imaging the May 2024 extreme aurora with ionospheric total electron content. *Geophysical Research Letters*, *51*, e2024GL111981. https://doi.org/10.1029/2024GL111981

Received 16 AUG 2024
Accepted 5 OCT 2024

Author Contributions:

Conceptualization: J. C. Foster
Formal analysis: J. C. Foster, P. J. Erickson, Y. Nishimura, S. R. Zhang
Funding acquisition: P. J. Erickson
Investigation: P. J. Erickson
Methodology: J. C. Foster, P. J. Erickson, Y. Nishimura, S. R. Zhang
Project administration: J. C. Foster

1. Introduction

For over 12 hr, the 10–11 May 2024 extreme Gannon geomagnetic storm sent brilliant auroral displays into the night skies at mid and low latitudes around the world. Extreme geomagnetic storms can have geospace system effects with negative societal impact (e.g., Baker et al., 2018; Knipp et al., 2016), including perturbations of the ionosphere that impact communications and navigation signals. In this report, we use the perturbation of satellite to ground navigation signals to map and quantify the increase in ionospheric total electron content (TEC) associated with the storm-induced energetic particle precipitation responsible for the evolving auroral display.

In the North American sector, cloudy skies obscured the view of the aurora from many locations, and the expansion of the storm's effects to unusually low latitudes took them out of range of many auroral-zone research facilities. Fortunately, the continental United States is increasingly well instrumented with facilities for mid-latitude upper atmosphere research that operate on a continuous basis. In addition, citizen scientists monitor and document the skies and can provide a wealth of information when unusual or unexpected events occur. We have combined ionospheric TEC data from distributed arrays of GNSS receivers, magnetometer chains, and citizen scientist all sky camera (ASC) imagery and auroral observations to provide a detailed view of the intense auroral breakup and westward surge at the peak of the May 2024 storm.

Resources: D. C. Bush, P. E. Meade, E. Franco-Diaz
Software: J. C. Foster, Y. Nishimura, S. R. Zhang
Supervision: J. C. Foster
Validation: J. C. Foster, P. J. Erickson, Y. Nishimura, S. R. Zhang, A. J. Coster
Visualization: J. C. Foster, P. J. Erickson, Y. Nishimura, S. R. Zhang, D. C. Bush
Writing – original draft: J. C. Foster, Y. Nishimura, S. R. Zhang
Writing – review & editing: J. C. Foster, P. J. Erickson, Y. Nishimura, S. R. Zhang, D. C. Bush, A. J. Coster, P. E. Meade, E. Franco-Diaz

2. Solar Drivers of the May 2024 Superstorm

During the first full week of May 2024, the large solar active region AR3664 emitted eight strong X-ray flares that launched a series of coronal mass ejections (CMEs) streaming toward Earth. On 10–11 May UT, a cluster of CME remnants arrived at Earth over a span of several hours creating an intense, long-lasting geomagnetic storm. As the first CME reached Earth near 17 UT on 10 May, solar wind dynamic pressure increased from 2 to >40 nPa. With the arrival of the second CME near 22 UT, the interplanetary magnetic field (IMF) magnitude increased to 70 nT with B_z decreasing to −50 nT. Solar wind and IMF observations at the Sun-Earth L1 point are shown in Figure S1 in Supporting Information S1.

3. Magnetospheric Response

Magnetospheric response to the May 2024 CMEs is shown in Figure 1. Following a brief positive spike when the first CME hit the magnetopause, the SYM-H geomagnetic disturbance index decreased steadily for 10 hr during the growth phase of the storm before spiking downward to a minimum of −500 nT at 02 UT on 11 May. At mid-latitudes, Computational Physics, Inc.'s NSF DASI program (Foster, 2006) Magstar magnetometers made continuous real-time 1 Hz cadence vector B field observations shown in Figure 1 that identify the onset of a strong ionospheric electrojet current over the continental US around 02:00 UT on 11 May. Along the East coast magnetometer chain (stations defined in Figure 1), a maximal *H*-component perturbation of −1,000 nT, accompanied by a sign change in *Z*-component localizing the electrojet, was seen at 02:06 UT centered over Westford, Massachusetts (42.6 N, 71.3 W). Simultaneously, along the midwest Magstar chain (stations defined in Figure 1), the electrojet intensification was centered over St. Bonifacius, Minnesota (44.9 N, 93.7 W), beginning there at 02:04 UT and reaching maximal H perturbation of −850 nT at 02:06 UT.

4. Auroral Observations

Auroral onset refers to the initial stage of an auroral substorm ($T = 0$), that is, the sudden brightening at or near a pre-existing active auroral arc prior to the poleward expansion of auroral activity (Akasofu, 1964). The onset for this substorm was first seen in Boston University all sky imager data between 02:00 and 02:02 UT (∼22 MLT) on 11 May at Millstone Hill, Massachusetts (42.6 N, 71.3 W; Figure S2 in Supporting Information S1), coinciding with the initiation of the electrojet enhancement in Figure 1. Auroral intensification extended westward to the central United States near 94 W longitude at 02:02 UT. A large expansion and southwestward propagation (auroral breakup) started at 02:05 UT (∼21 MLT). Clear skies prevailed in this region where the private Missouri Skies Observatory (40.25 N, 94.32 W) recorded color ASC and wide-angle color north-looking and B&W east-looking video with 1-s frame rate throughout the 11 May auroral event. Figures 2a–2c present three selected frames from the Missouri Skies ASC video showing this auroral sequence. North is at the top of the frames and twilight is seen on the west (right) horizon. Faint red aurora first appeared on the east horizon at 02:02:30 UT and green aurora expanded past the brightening red band and into the ASC zenith by 02:04:45 UT. The bright red band developed a structured equatorward edge at 02:06:00 UT with a mixture of structured green emission and continued to expand equatorward into the ASC zenith by 02:10:00 UT.

Auroral photos taken from a 3,200-foot (975 m) altitude along the Blue Ridge Parkway (37.93 N, 78.95 W) looking WNW over Staunton, Virginia recorded the evolution of the equatorward edge of the auroral oval during the 02 UT event. Figure 2d taken at 02:06 UT (photo credit Dave Lyons) shows a bright red auroral feature embedded in the green aurora at the equatorward edge of strong red aurora (using Nikon Z8 with 14 mm lens at 1.6 s, f3.2, ISO 1000). The photographer recorded a continuous sequence of 1.6, 3, and 6 s exposures at the time. This bright structure was not present in his frames at 02:04 UT and began to develop at 02:05 UT. The strong red emission at higher altitude, with weaker green emission below, suggests that the emission was driven by soft (100 s eV) electron precipitation. Surrounding green emissions indicate higher-energy (keV) electron precipitation. Other Virginia photographers posted photos of this feature taken from a variety of locations. Moonset for Staunton, Virginia was at 02:40 UT on 11 May. The ∼8 deg moon elevation angle in these photos, combined with the ∼1/4 deg/min rotation of the celestial sphere, indicates that they were taken near 02:08 UT, providing additional views of this auroral structure and its evolution.

North color and East-looking B&W wide-angle video frames and still photos from the Missouri Skies site (Figure S3 in Supporting Information S1) recorded a similar bright red structured feature as auroral breakup expanded past 40 N latitude between 02:08 and 02:10 UT. The line-of-sight distance between the Virginia and Missouri

10.1029/2024GL111981

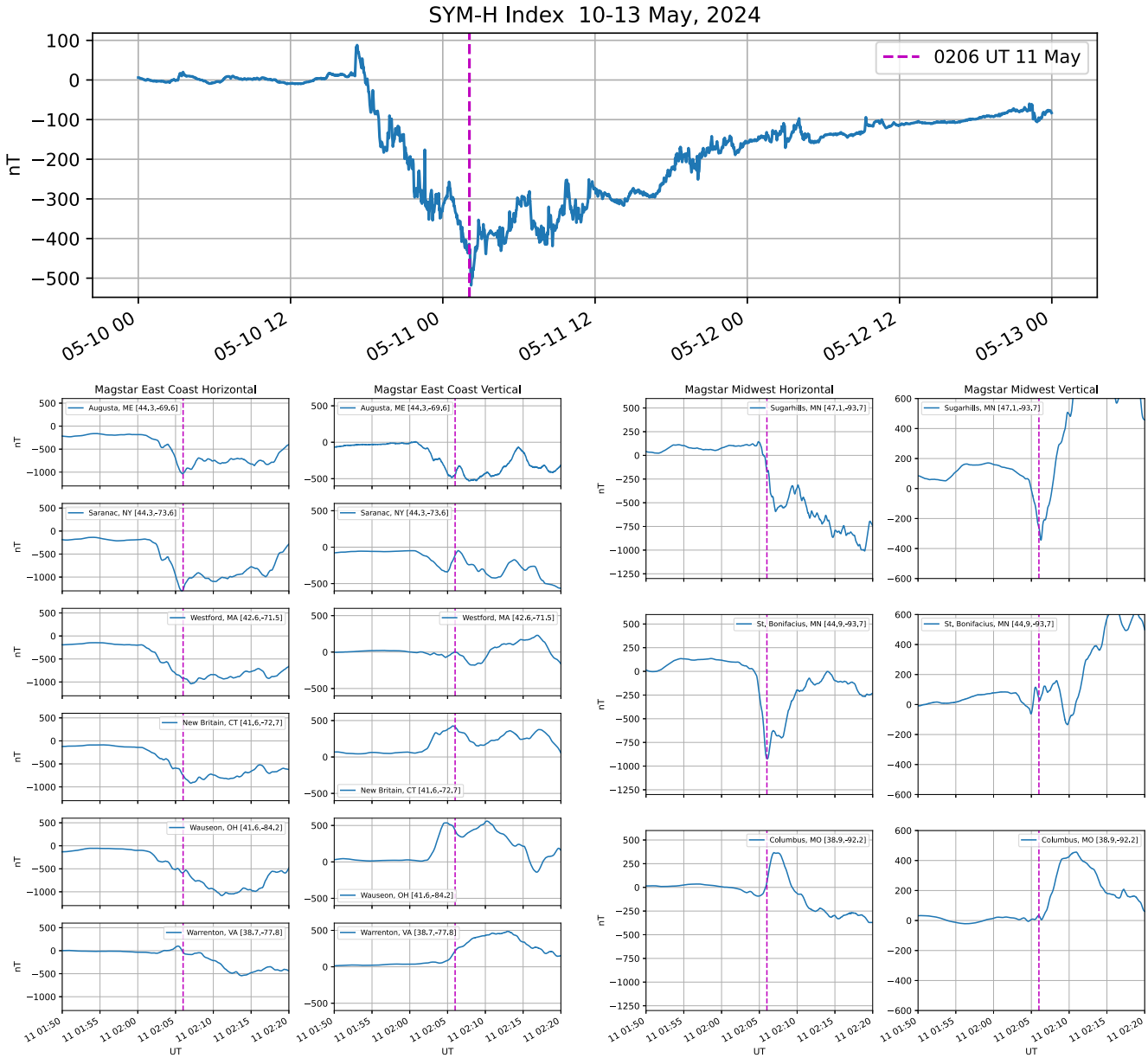

Figure 1. (upper) SYM-H for 10–11 May 2024 UT. Storm growth phase maximum occurred at 02:06 UT 11 May (indicated by the dashed vertical line in all Figure 1 plots). (lower) *H* and *Z* component mid-latitude magnetometer measurements from the east coast and midwest Computational Physics, Inc. MagStar chains on 11 May 2024. The St. Bonifacius, MN site is nearly under the auroral breakup point identified in the total electron content data. The Columbus MO magnetometer is a degree south of the all sky camera (ASC) site. Zero crossing of the *Z* component (e.g., electrojet overhead) in both chains at 02:10 UT corresponds to the time that strong aurora reached the zenith in the ASC imagery.

observing sites is 1,600 km and the horizon at 230-km altitude from the Virginia site is 1,730 km. It is possible that similar auroral structure formed or extended along the advancing edge of the red aurora across a wide extent of longitude.

5. Imaging Extreme Aurora With TEC

Ionospheric TEC from distributed arrays of GNSS receivers has been used in a wide variety of geospace investigations including storm-time ionospheric perturbations (Foster & Rideout, 2005), magnetosphere-ionosphere coupling effects (Foster et al., 2002; Walsh et al., 2014), and eclipse-induced effects (Coster et al., 2017; Zhang et al., 2017). Watson et al. (2011) used GPS TEC to investigate the evolution of substorm

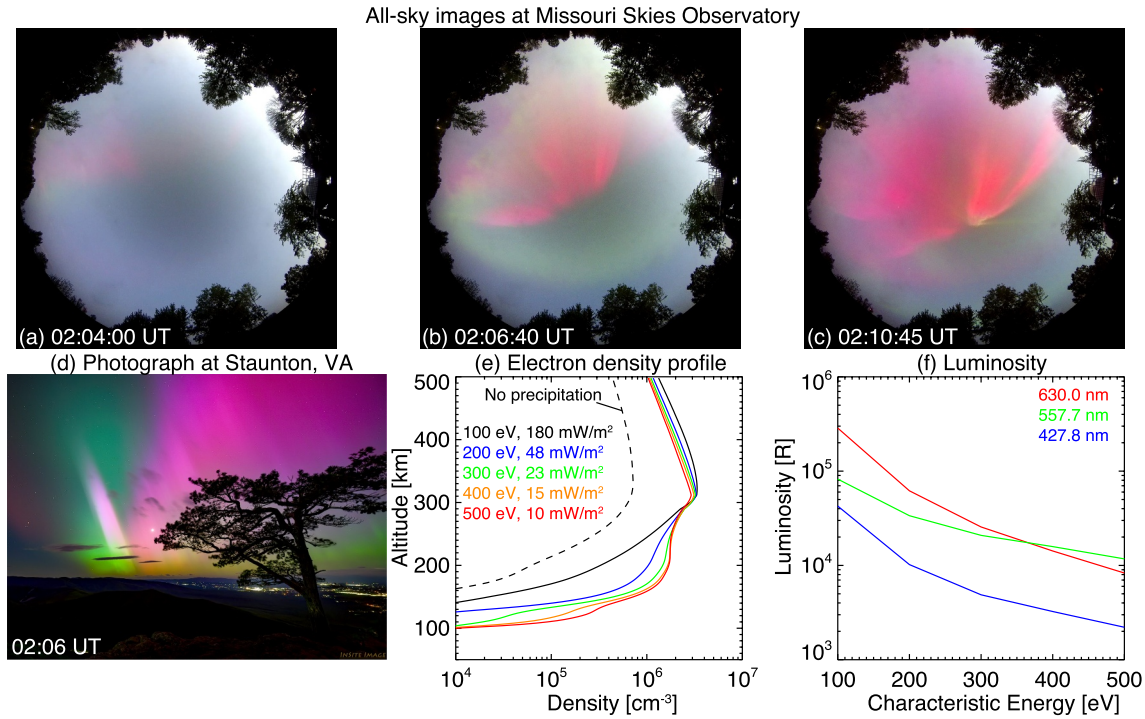

Figure 2. (a–c) Selected frames from the video recorded by the all-sky camera at Missouri Skies Observatory. North is to the top and west is to the right. (d) Photograph taken near Staunton, VA at 02:06 UT, looking westward (photo credit Dave Lyons). (e) Electron density profiles using the Fang et al. (2010) model and the Maxwellian distribution. The precipitating flux and characteristic energies are shown in the panel. (f) The auroral luminosities at the 630.0, 557.7, and 427.8 nm wavelengths using the Global Airglow Model model for these precipitation parameters.

particle precipitation at auroral latitude. Spogli et al. (2024) have addressed ionospheric space weather effects of the May 2024 superstorm over the Mediterranean sector including a pronounced negative ionospheric storm registered in TEC and a significant equatorward displacement of the main ionospheric trough.

5.1. TEC Auroral Mapping

We generate continental maps of vertical TEC (vTEC) derived from line of sight measurements between individual GNSS receiver site and satellite pairs filtered to retain data with satellite elevation angle >50 deg. One-minute median values of TEC within 1 × 1 latitude versus longitude grids are calculated for a 150 km altitude ionosphere penetration point (IPP) over the auroral impact region. We plot differential TEC by subtracting 5-min median pre-breakup values (01:55 UT–01:59 UT). In Figure 3, a sequence of maps depicts the development of the auroral breakup at 02:06 UT on 11 May 2024. Black circles denote the locations of the Missouri Skies Observatory and the Virginia auroral observing sites. Auroral TEC brightening of 5–10 TECu (1 TECu = 10^{16} electrons/m^2) began over the northeastern United States around 02:04 UT and spread to the Midwest by 02:06 UT as seen in the magnetometer data of Figure 1. The auroral breakup took place near 94 W longitude and spread poleward and equatorward while surging westward along the auroral oval (evident at 02:08 UT and thereafter). Median TEC enhancement near the center of the breakup (44 N, 94 W) ranged from 20 to 40 TECu while intensifications along the expanding auroral oval were 15–25 TECu.

We have extracted images from the Missouri Skies color ASC videos and mapped them to the ionosphere with the red channel intensity projected to 230 km altitude (a typical altitude for precipitation at a few 100 s eV). The black curves on each frame in Figure 3 mark the leading edge of the red aurora at the corresponding time (ASC mapping for 02:08:00 UT is shown in Figure S4 in Supporting Information S1) The westward and equatorward propagation of the red aurora matches well with the development of the overall TEC enhancement. For the red aurora, the westward speed was ∼2 km/s and the southward speed ∼0.5 km/s. Auroral TEC enhancement spreads into the zenith of Missouri ASC by 02:10 UT, as seen in Figure 2c. Based on the direct auroral observations, we believe

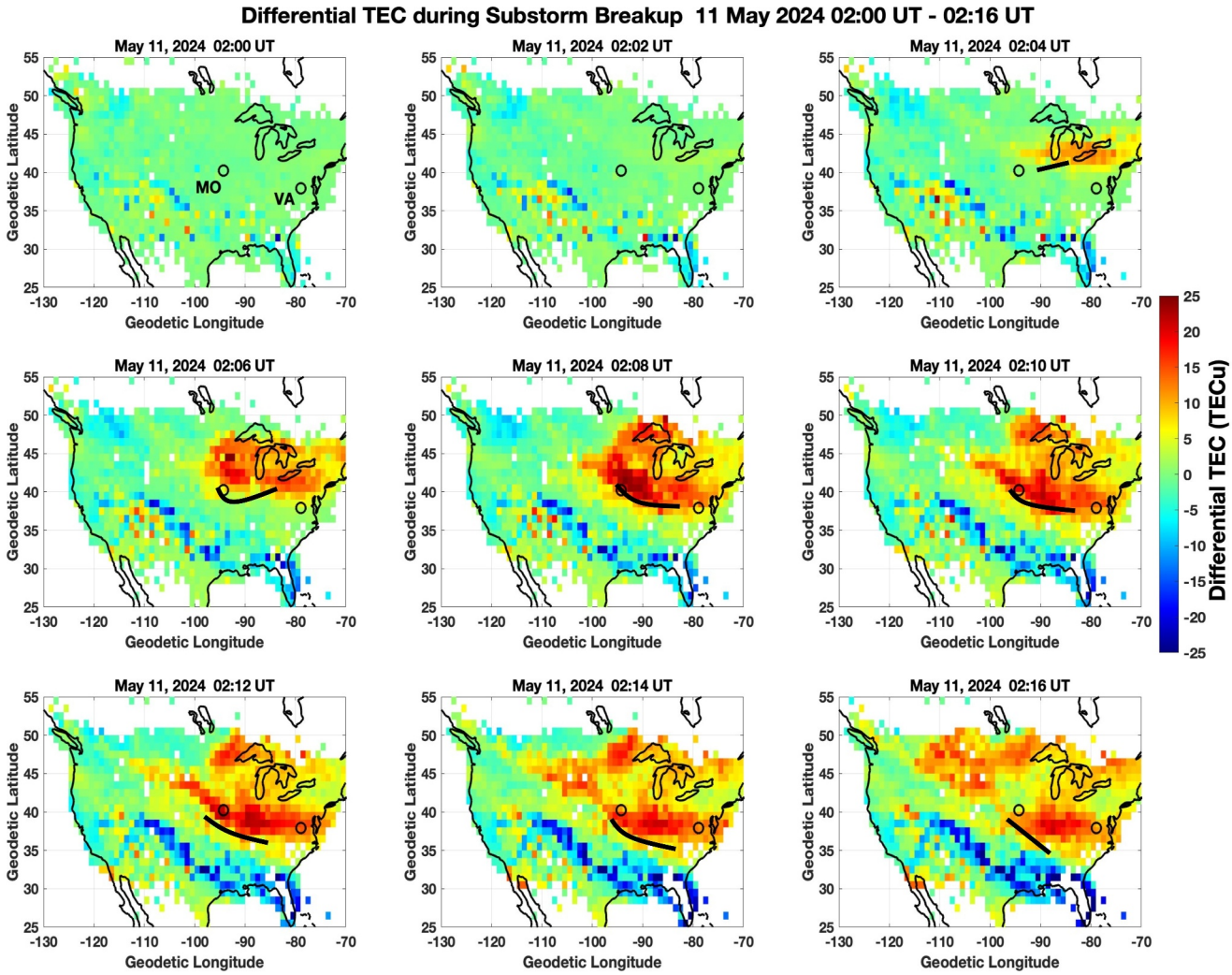

Figure 3. Median differential line of sight vTEC in 1 × 1 lat × lon grid for 1-min data samples from 02:00 UT to 02:16 UT on 11 May 2024. (Elevation angle >50 deg. 150 km IPP). Open circles denote locations of the Missouri Skies optical observatory (MO) and the Raven's Roost observing position (VA). Black curves mark the equatorward boundary of the strong red aurora derived from the MO all sky camera imagery.

that the westward expansion of low-energy electron precipitation is likely the driver of the large TEC enhancements observed during the event.

5.2. TEC Bursts at Auroral Breakup

During a 2-min interval (02:06–02:07 UT) coincident with the auroral breakup, individual receiver/satellite data sets indicated sharp bursts of greatly elevated vTEC. Examples of these 30-s cadence burst observations are presented in the lower portion of Figure 4. In aggregate, we recorded 35 separate bursts of vTEC >60 TECu for satellite/receiver pairs with elevation angle >62.5 deg. The median value of these TEC bursts was 70 TECu, some 50 TECu above the storm-enhanced background. The bursts were highly clustered around the point of auroral breakup in latitude, longitude, and time (see Figure S5 in Supporting Information S1 for details). Burst locations assuming a 150 km ionospheric penetration point (IPP) are indicated by white stars overplotted on the vTEC map for 02:07 UT in the upper left portion of Figure 4. (Because of the high elevation angle (>62.5 deg) selection criterion, the latitude/longitude distribution of burst points is not significantly different for a 230 km IPP.) The upper right portion of Figure 4 depicts the temporal evolution of median value differential vTEC in a 1 × 1 lat/long grid along the 94 W meridian. Samples of the strong TEC bursts increase the median differential vTEC values to >30 TECu in the 02:06–02:08 UT time interval (see Figure S5b in Supporting Information S1).

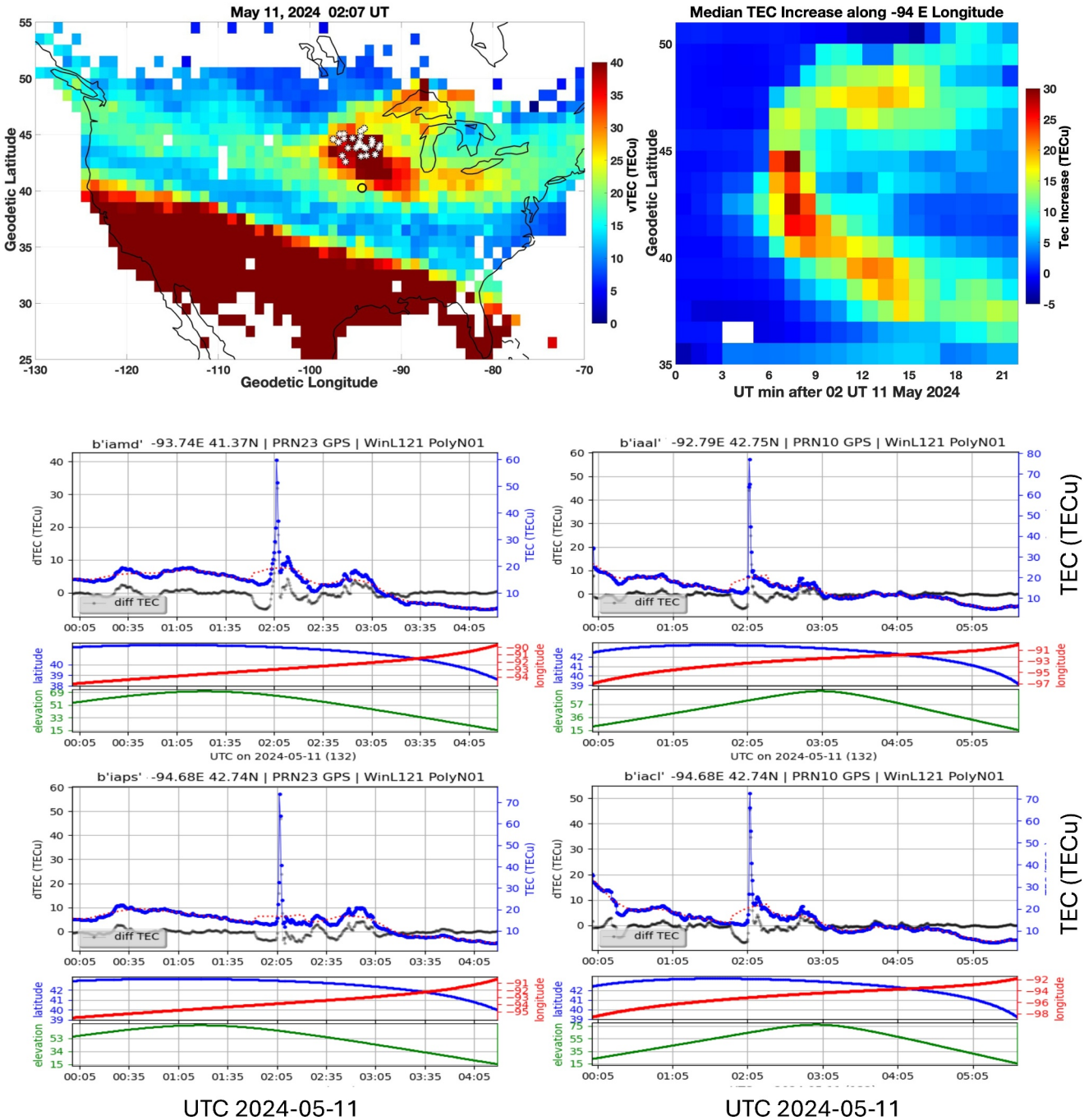

Figure 4. (top left) Median total vTEC map showing the spatial concentration of the 35 high elevation total electron content (TEC) bursts (el > 62.5 deg; white stars) observed over the 2-min interval 02:07–02:08 UT. (150 km IPP used for mapped data.) Open circle denotes location of Missouri optical observatory. (top right) Median differential vTEC and N-S expansion along 94 W longitude during the auroral breakup event. (bottom) TEC bursts: Four representative single satellite - single ground station plots of vTEC are shown displaying sharp bursts at 02:05 UT. (upper panels) total vTEC (blue), differential TEC (gray). (lower panels) Spacecraft latitude (blue), longitude (red), elevation angle from ground station (green).

6. Discussion

6.1. Precipitation Estimates

The sharp leading edge of the aurora was the brightest, and intense precipitation there may explain the TEC spikes detected at the onset of the auroral breakup. For the spatial/temporal region where the TEC bursts were observed

(43–45 N lat, 92–94 W lon, 20:06–02:08 UT) there were 190 vTEC observations with >30 deg elevation angle. We find that bursts with vTEC >55 TECu were ∼4 times more likely to be observed at high elevation angles 50–70 deg (20 of 101 samples) than at 30–50 deg (5 of 89 samples). This suggests that the TEC bursts were associated with temporally or spatially discrete field-aligned precipitation features. A higher (more field-aligned) elevation angle would sample a greater altitude extent of a spatially-discrete field-aligned high-TEC feature. With a constraint that the TEC bursts are created by precipitating electron flux sufficient to produce a 50 TECu enhancement, guided by the color and intensity of the co-located aurora, we estimate the characteristics of the burst precipitation associated with the auroral breakup during this extreme event.

The night sky has an intensity of about 250 R (1 Rayleigh = 10^{10} photons $m^{-2}s^{-1}$), while auroras can reach values of 1,000 kR (Hunten, 1955). A Class III 5577A green aurora with the 100 kR brightness of a moonlit cumulus cloud would entail a precipitating energy flux of ∼300 mW m^{-2} (Hultqvist, 1964). Figure 2e shows the calculated electron density profiles in Missouri at 2 UT for electron precipitation with a Maxwellian distribution with characteristic energies between 100 and 500 eV using the Fang et al. (2010) model. The ionization rate in Fang et al. (2010) is parameterized as described in their Section 3. MSIS (Picone et al., 2002) is used to obtain the neutral density and temperature as input parameters to their Equations 1 and 2. The recombination rate uses the formulas by Brekke (2013), as functions of the neutral density and temperature. The energy fluxes indicated for each characteristic energy are chosen to create a 50 TECu increase above the background (no precipitation, dashed line). The auroral luminosities at 630.0, 557.7, and 427.8 nm wavelengths are calculated using these precipitation parameters using the Global Airglow Model (GLOW, Solomon, 2017) (Figure 2f). Precipitation below ∼300 eV characteristic energy creates auroral emission that is dominated by the red color. Considering the mixture of the red and green emission in Figure 2c, it is likely that the characteristic energy is around 200–300 eV. The modeled luminosities close to 100 kR are fairly bright compared to typical nightside aurora at high latitudes, explaining why the aurora was visible even during twilight. The 23–48 mW/m^2 energy fluxes also are intense and very unusual at mid-latitudes. The soft electron precipitation creates electron density enhancements above ∼120 km altitude with a peak at ∼300 km, indicating that the precipitation has a large impact in the *F*-region ionosphere.

6.2. TEC Accuracy

Following the procedure described by Rideout and Coster (2006) and Vierinen et al. (2016), we use pseudo range data to determine the TEC absolute value. The pseudo range is a measurement of the delay difference between the different frequencies of the L1 and L2 signals. Because pseudo range measurement is quite noisy (3–5 TECu variability), the carrier phase typically is used to smooth the TEC values. During the burst event, multiple different makes of receivers accurately tracked the pseudo range data across the TEC bursts, all seeing a large increase in TEC as shown in Figure 4. Single site vTEC values from line-of-sight slant TEC measurements at the 150 km IPP, as shown in the bottom panels in Figure 4, demonstrate how several different receivers track these TEC spikes. However, the carrier phase data did not track across the sharp increase, with the result that error bars around the sudden spikes in TEC were larger (3–5 TECu) because of uncompensated noise in the pseudo-range measurements. Here we consider only high elevation data and estimate the error due to noise in the pseudo range measurements to be ∼3 TECu.

6.3. Prior TEC Burst Observations

Watson et al. (2011) used TEC to track the evolution of substorm particle precipitation at auroral latitudes using TEC from individual receiver station—satellite pairs. They reported sharp precipitation-produced TEC increases of 5–10 TECu over background (with 2–3 min duration) at substorm onset on select satellite-receiver paths. Zou et al. (2009) report an ionization spike reaching 10^{12} m^{-3} at 120 km altitude associated with the equatorward portion of the auroral spiral and its later expansion. For a super substorm at auroral latitude, Nishimura et al. (2020) reported that substorm auroral onset was accompanied by a large TEC enhancement reaching 38 TECu (a 20 TECu increase in 2 min). Chernyshov et al. (2020) determined that sharp jumps in TEC are related to substorm precipitation, occurring in the vicinity of the equatorward boundary of the auroral oval. Prikryl et al. (2021) observed substorm increases of 10–15 TECu at auroral latitudes and show spike-like vTEC increases of 10–15 TECu at the onset of auroral breakup.

7. Summary

The highly unusual May 2024 superstorm presents a broad potential for new geospace insight and discoveries (e.g., the apparent merging of the southern crest of the equatorial ionization anomaly with the aurora, Karan et al., 2024, or the injection of energetic protons into the proton radiation belt, Pierrard et al., 2024). Widespread mid-latitude ionospheric effects were observed in the Asian sector (Guo et al., 2024) and Europe (Spogli et al., 2024). Here we have focused on the increase in ionospheric TEC associated with the storm-induced energetic particle precipitation responsible for the evolving extreme auroral display.

TEC maps show the intensification and spread of the 11 May 2024 02 UT extreme auroral event across the continental US over a 20-min interval. The auroral TEC enhancement was co-located with a 1,000 nT intensification of the electrojet current system. Mapping ASC images into geodetic coordinates at 230 km altitude, we find that the westward and equatorward propagation of strong red aurora matches well with the development of the overall TEC enhancement.

During a 2-min interval coincident with the auroral breakup, individual receiver/satellite data sets indicated sharp bursts of greatly elevated vTEC (50 TECu above background). The bursts were seen predominantly at high elevation angles (>50 deg) suggesting that they were associated with temporally or spatially discrete field-aligned precipitation features.

Auroral breakup was accompanied by a bright red over green discrete auroral feature at the leading edge of the equatorward expansion of strong red aurora. Based on the direct auroral observations, we believe that the westward expansion of low-energy electron precipitation is likely the driver of the large TEC enhancements observed during the event. We estimate a characteristic energy of ∼200–300 eV with 23–48 mW/m^2 energy flux for soft electron precipitation capable of producing a 50 TECu enhancement at the onset of the auroral breakup.

Data Availability Statement

Data processing used SPEDAS software (https://spedas.org/) (Angelopoulos et al., 2019).

The Fang et al. (2010) model and GLOW model software is available at: https://github.com/fgasdia/EPPIonization.jl, https://pypi.org/project/glowpython/.

DISCOVR data is available through the DISCOVR Space Weather Data Portal at: https://www.ngdc.noaa.gov/dscovr/portal/index.html#/.

Missouri Skies all-sky camera video, Magstar magnetometer data, and line-of sight total electron content (TEC) data included in this study, along with software used in data processing and figure generation are available at: Haystack Observatory et al. (2024).

Acknowledgments
JF and DB received no financial support for work on this study. The work of YN was supported by NASA Grants 80NSSC20K0725, 80NSSC21K1321, 80NSSC22K0323, 80NSSC22K0749, 80NSSC23M0193, and 80NSSC23K0410, NSF Grants AGS-1907698 and AGS-2100975, and AFOSR Grants FA9550-23-1-0614 and FA9550-23-1-0634. GNSS TEC data processing and Madrigal database system are provided to the community by MIT under NSF Grant AGS-1952737 support. This work was supported by NASA Grants 80GSFC22CA011, 80NSSC21K1310, 80NSSC22K0171, 80NSSC22K1013, 80NSSC19K0078, NSF Grants AGS-2033787, AGS-2149698, and ONR Grant N00014-24-1-2122 and N00014-23-1-2160 Magstar installation and data distributions were supported by NSF AGS-1933040 and AGS-2242805. We thank Dave Lyons for the use of his auroral photography, Chris Kridler for sharing auroral photos, and ISSI/ISSJ-BJ through ISSI International Team projects Multi-Scale Magnetosphere-Ionosphere-Thermosphere Interaction, Auroral Research Coordination: Towards Internationalized Citizen Science (ARCTICS), and Magnetotail Dipolarizations: Archimedes Force or Ideal Collapse?.

References

Akasofu, S.-I. (1964). The development of the auroral substorm. *Planetary and Space Science*, *12*(4), 273–282. https://doi.org/10.1016/0032-0633(64)90151-5

Angelopoulos, V., Cruce, P., Drozdov, A., Grimes, E. W., Hatzigeorgiu, N., King, D. A., et al. (2019). The space Physics environment data analysis system (SPEDAS) [Software]. *Space Science Reviews*, *215*(1), 9. https://doi.org/10.1007/s11214-018-0576-4

Baker, D. N., Erickson, P. J., Fennell, J. F., Foster, J. C., Jaynes, A. N., & Verronen, P. T. (2018). Space weather effects in the Earth's radiation belts. *Space Science Reviews*, *214*(1), 17. https://doi.org/10.1007/s11214-017-0452-7

Brekke, A. (2013). *Physics of the upper polar atmosphere*. Springer Verlag. https://doi.org/10.1007/978-3-642-27401-5

Chernyshov, A. A., Miloch, W. J., Jin, Y., & Zakharov, V. I. (2020). Relationship between TEC jumps and auroral substorm in the high-latitude ionosphere. *Scientific Reports*, *10*(1), 6363. https://doi.org/10.1038/s41598-020-63422-9

Coster, A. J., Goncharenko, L., Zhang, S.-R., Erickson, P. J., Rideout, W., & Vierinen, J. (2017). GNSS observations of ionospheric variations during the 21 August 2017 solar eclipse. *Geophysical Research Letters*, *44*(24), 12041–12048. https://doi.org/10.1002/2017GL075774

Fang, X., Randall, C. E., Lummerzheim, D., Wang, W., Lu, G., Solomon, S. C., & Frahm, R. A. (2010). Parameterization of monoenergetic electron impact ionization [Software]. *Geophysical Research Letters*, *37*(22), L22106. https://doi.org/10.1029/2010GL045406

Foster, J. C. (2006). *DASI: Distributed arrays of small instruments for solar-terrestrial research*. U.S. National Research Council Workshop Report, National Academies Press. https://doi.org/10.17226/11594

Foster, J. C., Erickson, P. J., Coster, A. J., Goldstein, J., & Rich, F. J. (2002). Ionospheric signatures of plasmaspheric tails. *Geophysical Research Letters*, *29*(13), 1623. https://doi.org/10.1029/2002GL015067

Foster, J. C., & Rideout, W. (2005). Midlatitude TEC enhancements during the October 2003 superstorm. *Geophysical Research Letters*, *32*(12), L12S04. https://doi.org/10.1029/2004GL021719

Guo, X., Zhao, B., Yu, T., Hao, H., Sun, W., Wang, G., et al. (2024). East–west difference in the ionospheric response during the recovery phase of May 2024 super geomagnetic storm over the East Asian. *Journal of Geophysical Research: Space Physics*, *129*(9), e2024JA033170. https://doi.org/10.1029/2024JA033170

Haystack Observatory, Zhang, S., Foster, J., & Bush, D. (2024). Superstorm ionospheric observations in the continental US [collection]. *Zenodo*. https://doi.org/10.5281/zenodo.13328751

Hultqvist, B. (1964). *Aurora, Goddard energetic particles Preprint series, X-611-64-97*. NASA Goddard Space Flight Center. Retrieved from https://ntrs.nasa.gov/citations/19640018166

Hunten, D. M. (1955). Some photometric observations of auroral spectra. *Journal of Atmospheric and Terrestrial Physics*, *7*, 141–151. https://doi.org/10.1016/0021-9169(55)90121-5

Karan, D. K., Martinis, C. R., Daniell, R. E., Eastes, R. W., Wang, W., McClintock, W. E., et al. (2024). GOLD observations of the merging of the Southern Crest of the equatorial ionization anomaly and aurora during the 10 and 11 May 2024 Mother's Day super geomagnetic storm. *Geophysical Research Letters*, *51*(15), e2024GL110632. https://doi.org/10.1029/2024gl110632

Knipp, D. J., Ramsay, A. C., Beard, E. D., Boright, A. L., Cade, W. B., Hewins, I. M., et al. (2016). The May 1967 great storm and radio disruption event: Extreme space weather and extraordinary responses. *Space Weather*, *14*(9), 614–633. https://doi.org/10.1002/2016SW001423

Nishimura, Y., Lyons, L. R., Gabrielse, C., Sivadas, N., Donovan, E. F., Varney, R. H., et al. (2020). Extreme magnetosphere-ionosphere-thermosphere responses to the 5 April 2010 supersubstorm. *Journal of Geophysical Research: Space Physics*, *125*(4), e2019JA027654. https://doi.org/10.1029/2019JA027654

Picone, J. M., Hedin, A. E., Drob, D. P., & Aikin, A. C. (2002). NRLMSISE-00 empirical model of the atmosphere: Statistical comparisons and scientific issues. *Journal of Geophysical Research*, *107*(A12), 1468. https://doi.org/10.1029/2002JA009430

Pierrard, V., Winant, A., Botek, E., & Péters de Bonhome, M. (2024). The Mother's Day solar storm of 11 May 2024 and its effect on Earth's radiation belts. *Preprints*, *2024*, 2024091134. https://doi.org/10.20944/preprints202409.1134.v1

Prikryl, P., Weygand, J. M., Ghoddousi-Fard, R., Jayachandran, P. T., Themens, D., McCaffrey, A., et al. (2021). Temporal and spatial variations of GPS TEC and phase during auroral substorms and breakups. *Polar Science*, *28*, 100602. https://doi.org/10.1016/j.polar.2020.100602

Rideout, W., & Coster, A. (2006). Automated GPS processing for global total electron content data. *GPS Solutions*, *10*(3), 219–228. https://doi.org/10.1007/s10291-006-0029-5

Solomon, S. C. (2017). Global modeling of thermospheric airglow in the far ultraviolet [Software]. *Journal of Geophysical Research: Space Physics*, *122*(7), 7834–7848. https://doi.org/10.1002/2017JA024314

Spogli, L., Alberti, T., Bagiacchi, P., Cafarella, L., Cesaroni, C., Cianchini, G., et al. (2024). The effects of the May 2024 Mother's Day superstorm over the Mediterranean sector: From data to public communication. *Annals of Geophysics*, *67*(2), PA218. https://doi.org/10.4401/ag-9117

Vierinen, J., Coster, A. J., Rideout, W. C., Erickson, P. J., & Norberg, J. (2016). Statistical framework for estimating GNSS bias. *Atmospheric Measurement Techniques*, *9*(3), 1303–1312. https://doi.org/10.5194/amt-9-1303-2016

Walsh, B. M., Foster, J. C., Erickson, P. J., & Sibeck, D. G. (2014). Simultaneous ground and space-Based observations of the plasmaspheric Plume and magnetospheric reconnection. *Science*, *343/6175*, 1122–1125. https://doi.org/10.1126/science.1247212

Watson, C., Jayachandran, P. T., Spanswick, E., Donovan, E. F., & Danskin, D. W. (2011). GPS TEC technique for observation of the evolution of substorm particle precipitation. *Journal of Geophysical Research*, *116*(A10), A00I90. https://doi.org/10.1029/2010JA015732

Zhang, S.-R., Erickson, P. J., Goncharenko, L. P., Coster, A. J., Rideout, W., & Vierinen, J. (2017). Ionospheric bow waves and perturbations induced by the 21 August 2017 solar eclipse. *Geophysical Research Letters*, *44*(24), 12067–12073. https://doi.org/10.1002/2017GL076054

Zou, S., Lyons, L. R., Nicolls, M. J., Heinselman, C. J., & Mende, S. B. (2009). Nightside ionospheric electrodynamics associated with substorms: PFISR and THEMIS ASI observations. *Journal of Geophysical Research*, *114*(A12), A12301. https://doi.org/10.1029/2009JA014259